

An overview on development and application of an experimental platform for quantitative cardiac imaging research in rabbit models of myocardial infarction

Yuanbo Feng, Jan Bogaert, Raymond Oyen, Yicheng Ni

KU Leuven, Department of Imaging and Pathology, Theragnostic Laboratory, Radiology Section, University Hospital Gasthuisberg, Leuven, Belgium

Correspondence to: Prof. Dr. Yicheng Ni, MD, PhD. Radiology Section, University Hospitals, KU Leuven, Herestraat 49, 3000 Leuven, Belgium. Email: yicheng.ni@med.kuleuven.be.

Abstract: To exploit the advantages of using rabbits for cardiac imaging research and to tackle the technical obstacles, efforts have been made under the framework of a doctoral research program. In this overview article, by cross-referencing the current literature, we summarize how we have developed a preclinical cardiac research platform based on modified models of reperfused myocardial infarction (MI) in rabbits; how the *in vivo* manifestations of cardiac imaging could be closely matched with those *ex vivo* macro- and microscopic findings; how these imaging outcomes could be quantitatively analyzed, validated and demonstrated; and how we could apply this cardiac imaging platform to provide possible solutions to certain lingering diagnostic and therapeutic problems in experimental cardiology. In particular, tissue components in acute cardiac ischemia have been stratified and characterized, post-infarct lipomatous metaplasia (LM) as a common but hardly illuminated clinical pathology has been identified in rabbit models, and a necrosis avid tracer as well as an anti-ischemic drug have been successfully assessed for their potential utilities in clinical cardiology. These outcomes may interest the researchers in the related fields and help strengthen translational research in cardiovascular diseases.

Keywords: Rabbit; myocardial infarction (MI); cardiac imaging; histology; contrast

Submitted Aug 15, 2013. Accepted for publication Sep 05, 2013.

doi: 10.3978/j.issn.2223-4292.2013.09.01

View this article at: <http://dx.doi.org/10.3978/j.issn.2223-4292.2013.09.01>

Introduction

In translational medicine, animal models mimicking human diseases have made great contributions to the progress in the elucidation of physiological and pathophysiological mechanisms and development of new diagnostic and therapeutic approaches to these diseases including ischemic heart disease (IHD).

IHD is a leading cause of death worldwide and its cardiovascular consequences depend on complex multi-factorial pathologies, in which both genetic and environmental factors are implicated, thus making them very difficult to understand and manage. Making animal models of human IHD may provide us with critical insights

into pathophysiology and serve as essential tools for evaluation of new strategies to predict, treat and prevent these consequences.

Owing to its low cost, amazing fertility, and ease of handling and housing, the rabbit has been one of the most commonly used experimental animals. However, despite a number of theoretical advantages including clinically relevant cardiac dimension and beating rate, not until recently could the rabbit be routinely applied in cardiac imaging research due to the following technical challenges. First, myocardial infarction (MI) proved problematic to induce in rabbits because of their characteristic upper airway anatomy that hinders tracheal intubation and subsequent thoracic surgery for coronary artery (CA) intervention.

Secondly, unlike large animals such as pigs and dogs and small animals such as rats and mice, rabbits have not found a readily available standard method for making models of MI. Third, clinical imaging modalities such as magnetic resonance imaging (MRI) and single photon emission computer tomography (SPECT) had to be adapted for *in vivo* scanning beating heart in rabbits.

In vivo cardiac imaging techniques include echocardiography, MRI, SPECT, computed tomography (CT), positron emission tomography (PET), optical imaging and their various hybrid forms. They help assess myocardial viability after the MI in both acute and chronic settings by covering several aspects including cardiac morphology, left ventricular (LV) function, coronary perfusion, and myocardial metabolism (1). Each technique has the ability to assess one or more of these aspects for offering valuable diagnostic, prognostic and therapeutic information to facilitate clinical decision making (2-4).

With the development of small animal imaging modalities such as high magnet-field MRI, micro-PET and micro-SPECT, non-invasive imaging in small living animal models has gained increasing importance in preclinical research (5,6). However, these newly miniaturized imagers are expensive, difficult to handle and lacking robust post-processing software, and thus still remain challenging and non-standardized for wide applications.

There have been numerous studies in various animal models to mimic the reduction in coronary artery (CA) blood flow leading to abnormal myocardial functions and eventual occurrence of MI (7,8). Scientists are in search of magic bullets or drugs that can alleviate coronary symptoms, reduce infarct size and improve the recovery of contractile function. These endeavors have confronted significant challenges, since the proper imaging biomarkers crucial for early detection and progression prediction of these pathologies are yet poorly explored.

To tackle the above-specified obstacles and to exploit the advantages of using rabbits for cardiac imaging research, a series of efforts have been made under the framework of a doctoral research program as shown in the flowchart of *Figure 1*. In this mini-review, by cross-referencing the current literature, we summarize stepwise how we have developed a preclinical cardiac research platform based on an established reperfused MI model in rabbits by overcoming numerous technical constrains; how the *in vivo* manifestations of cardiac imaging based on the use of clinical imagers could be closely mirrored with those *ex vivo* macroscopic and microscopic findings; and how these

imaging outcomes could be quantitatively analyzed, validated and demonstrated. We have also exemplified the applications of this cardiac imaging platform for providing possible solutions to certain lingering diagnostic and therapeutic problems in experimental cardiology. In particular, tissue components in acute cardiac ischemia have been stratified using newly invented multifunctional staining techniques, post-infarct lipomatous metaplasia (LM) as a common but hardly elucidated pathology has been identified in rabbit models, and a necrosis avid tracer and an anti-ischemic drug have been successfully assessed for their potential diagnostic and therapeutic utilities. Given this newly developed preclinical cardiac imaging research platform, today hopefully it becomes more workable to devise and test more robust strategies against human cardiovascular diseases.

Developing a rabbit model of reperfused MI

In vivo cardiovascular research in clinically relevant animal models bridges the *in vitro* studies of cell culture and biochemical assays with the authentic more resource- and time-consuming clinical practice. Considering the greater costs and stricter ethical regulations in human studies, a variety of large and small animal models of myocardial ischemia/reperfusion have been introduced particularly in combination with multiparametric imaging biomarkers to envisage the internal real-time events in experimental research (1,9).

Nowadays, pig and rodent models are dominating preclinical animal research on IHD. Small animal models provide considerable insights into human cardiac pathophysiology. Myocardial damage in rodent hearts can be induced by three procedures: surgical (10), pharmacological (11), or electrical (12) procedures. Whereas the pig is the more preferred large animal to model human heart diseases, because the coronary anatomy and collateral circulation are very similar between pigs and humans, and thus the ischemic lesions can be mutually predicted (7). Among several models of MI in pigs, the most widely used is the balloon occlusion of CA branch (13) as appose to relatively uncommon microembolization model in large animals (14). However, until recently the rabbit as a medium size animal has been seldom applied for MI imaging, but mainly used for coronary atherosclerosis research in high-cholesterol diet or low-density lipoprotein receptor-deficient rabbits (15).

Rabbit models are beneficial due to their low costs, high reproductivity, and ease of housing and handling during the experiment. Relative to rats and mice, their larger size greatly

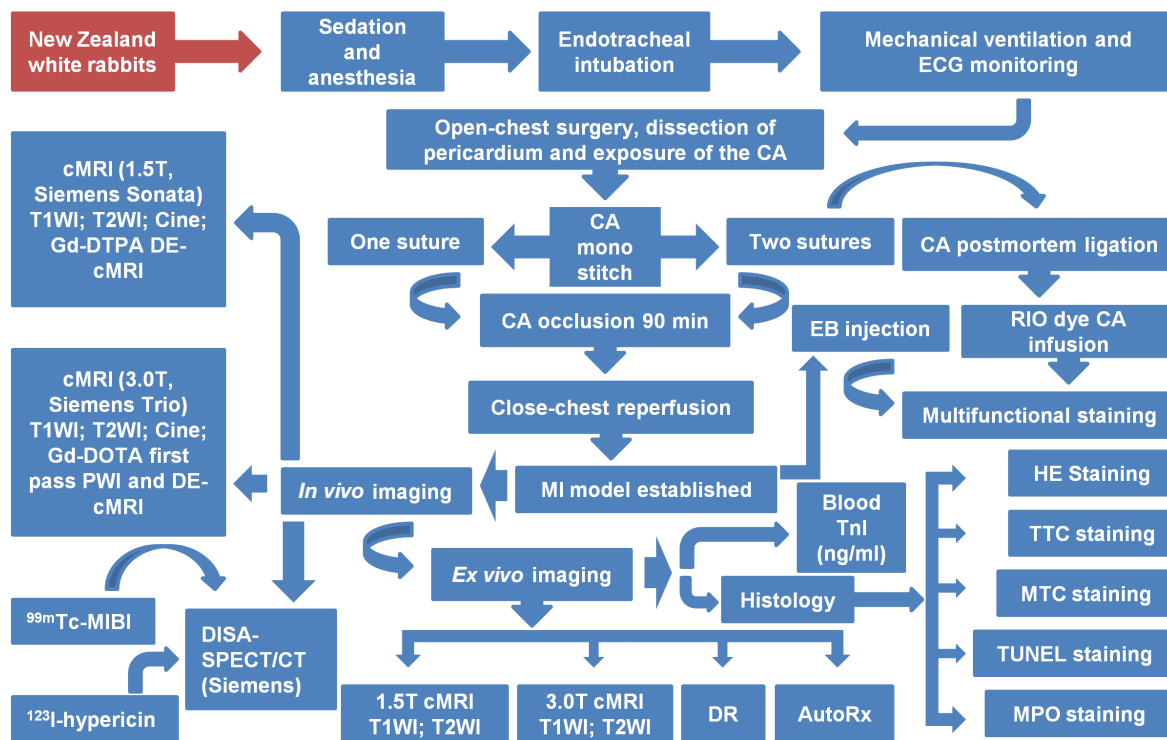


Figure 1 Flowchart of experimental cardiac imaging research in rabbits with myocardial infarction. Abbreviations: MI, myocardial infarction; CA, coronary artery; cMRI, cardiac magnetic resonance imaging; T1WI, T1 weighted imaging; T2WI, T2 weighted imaging; PWI, perfusion weighted imaging; DISA-SPECT/CT, dual-isotope simultaneous acquisition single photon emission computed tomography/computed tomography; MIBI, sestamibi; AutoRx, autoradiography; DR, digital radiography; EB, Evans blue; RIO, red iodized oil; TTC, triphenyltetrazolium chloride; HE, haematoxylin-eosin; MTC, Masson's trichrome; TUNEL, terminal deoxynucleotidyl transferase dUTP nick end labeling; MPO, myeloperoxidase; TnI, Troponin I.

facilitates surgical and postsurgical procedures. Comparing to larger animals, rabbits present lower risk of ventricular fibrillation after CA occlusion and reperfusion, leading to less drop-outs from the experiment (16). Recently, we have set up a novel rabbit model for cardiac MRI (cMRI) research on reperfused MI (9). The aim was to study the possibility of multiparametric cMRI and postmortem imaging for the evaluation of acute MI in rabbits.

The MI was induced by open-chest CA operation and close-chest CA reperfusion. Briefly, the procedure started with sedation or anesthesia, endotracheal intubation and mechanical ventilation, followed by the left 4-5th intercostal thoracotomy. After opening paricardium, the heart was slightly turned anticlockwise to expose the left circumflex (LCx) CA. A 2-0 silk suture was placed underneath the LCx at the level of 3 mm lower than the edge of the left atrial appendage and the MI was induced by tying the suture with a single knot with the detachable suture end from the knot left outside the thorax through the closed wound. Ninety minutes

after CA occlusion, a reperfused MI was induced by pulling the exteriorized suture end in the closed-chest condition, which re-opened the detachable knot. The following modifications have been made to ensure a successful operation and reduce animal mortality: (I) an easy method for blind transoral tracheal intubation was newly developed without needing a mechanical or optical laryngoscope; (II) the single-suture (non-snare loop) method allowed open-chest CA occlusion but close-chest CA reperfusion at ease; (III) the choice of LCx instead of left anterior descending (LAD) CA branch minimized occurrence of arrhythmia and guaranteed the quality of ECG gated cMRI; and (IV) *in vivo* cMRI was exactly co-localized with postmortem histochemically stained entire rabbit heart section on a standard glass slide (Figure 2). To further facilitate postmortem determination of the tissue components after myocardial ischemia, an approach with one stitch but two sutures was devised (17,18). Briefly, a sharp triangular needle of 1/2 circle with 2 spring eyes at the end (Sutura, Inc. Fountain Valley, CA, USA) was

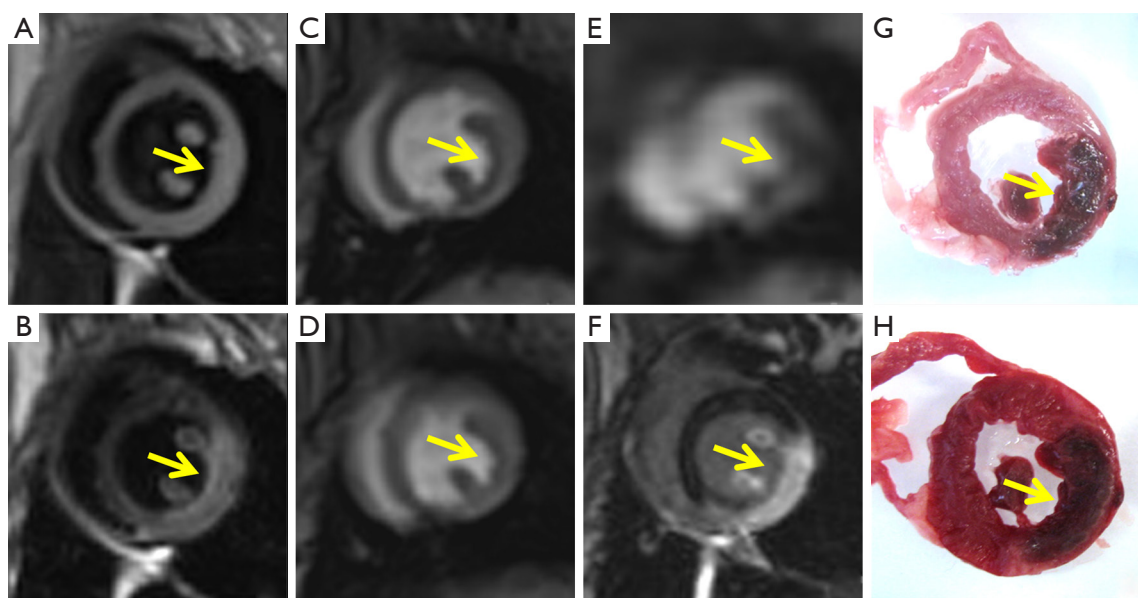


Figure 2 Cardiac MRI and histological findings in a rabbit with an acute transmural reperused myocardial infarction at the left circumflex coronary artery supplied territory involving both anterior and posterior papillary muscle. (A) On T1WI, the MI (arrow) appears isointense; (B) on T2WI, the lesion (arrow) appears hyperintense but somewhat larger than the real MI due to edema; (C,D) cine cMRI images at diastolic and systolic phase display no changes of the thickness at the LV wall with MI (arrow); (E) PWI image shows perfusion defect, suggesting the AAR (arrow) that appears larger than the real MI; (F) DE-cMRI depict the MI as a hyperenhanced zone (arrow); (G) fresh heart section shows hemorrhage at the MI (arrow); (H) TTC-stained heart section confirms this transmural hemorrhagic MI (arrow). MRI, magnetic resonance imaging; T1WI, T1 weighted imaging; MI, myocardial infarction; T2WI, T2 weighted imaging; cMRI, cardiac MRI; LV, left ventricular; PWI, perfusion weighted imaging; AAR, area at risk; TTC, triphenyltetrazolium chloride.

used (17). Two silk sutures could be easily placed through the separate eyes: the thicker 2-0 suture was used for the CA ligation that could be removed for reperfusion and the thinner 5-0 one was spared for later *ex vivo* CA re-occlusion in order to perform postmortem multifunctional stainings (see details in “Stratifying acute MI components in rabbits using multifunctional images”).

In summary, after technical optimization in several steps (Figure 1), the present experimental setup has enabled us to perform imaging-based cardiologic research in rabbits with enhanced applicability, accuracy and cost-effectiveness (9). This rabbit model of MI constitutes a fundamental part in the present preclinical platform for translational cardiac imaging research.

Applying cardiac MRI in rabbits with acute MI

Cardiac MRI is unique in its capability to offer several different methods for making prognosis regarding myocardial viability and predicting future cardiovascular events. These cMRI methods include dobutamine stress

cine- or tagging-MRI, perfusion MRI and delayed enhanced (DE) cMRI to assess contractile function or reserve, microvascular obstruction, and necrosis or scar characterization, respectively (19).

At present these advanced imaging methods have also been applied in studies on MI in small animals. For example, in a study on cardiac function in ischemic mice after *in vivo* administration of mesenchymal stem cells, using a 9.4 Tesla, Grauss *et al.* assessed the role of cMRI in characterizing this emerging technology when it starts to be incorporated in routine clinical practice (20). Despite the possible high-quality images derived from such cMRI, the use of high magnet-field imagers for cardiac ischemia research in small experimental animals is still very complicated and can be successful only after long and intensive endeavors. Measurement of MI by cMRI with clinical scanners can be more accurate in large animals, but they are more restricted ethically, and their heavy weight and noncompliance make it difficult to handle during cMRI procedures.

With the rabbit as medium-size animal model, its heart is about 10 and 100 times larger than that in rats and mice

respectively and 15-fold smaller than that from a human adult, but similar in size to that from a human infant. Such a cardiac dimension allows cMRI applications in both clinical MRI systems and moderately high magnet field (2.0-4.7 T) animal MRI systems. Rabbits have been reported for arrhythmogenic (21), coronary atherosclerotic (22) and other vascular imaging (23) researches. However, there have been few studies on imaging and evaluating IHD in rabbits using clinic MRI scanners.

In *Table 1*, the details about cMRI facilities and imaging acquisition parameters on rabbits with IHD are summarized. The majority of reported cMRI studies have been performed on 1.5 and 3.0 T MR scanners from Siemens and Philips (9,24-27). The spatial resolution of the cMRI ranged from 0.7 to 1.2 mm, which appears adequate for rabbit heart but insufficient for rats and mice. Barkhausen *et al.* and Mansencal *et al.* showed the highest spatial resolution of 0.7 mm on 1.5 T scanner, which seems even higher than that from a 3.0 T scanner (24,25). Recently Hu *et al.* published their results on quantitative cMRI assessment of ventricular remodeling in rabbit models with MI, though the real cardiac MR images failed to be convincingly demonstrated (28,29). In theory, the 3.0 T superconducting system with a higher magnetic field and the upgraded hardware and software should enable obtaining cMRI with higher signal-to-noise ratio (SNR), temporal and spatial resolutions, and speed of imaging acquisition as compared to the 1.5 T systems (30).

Earlier we have reported a rabbit myocardial ischemia-reperfusion model studied using a clinical 1.5 Tesla scanner (9), which was positively introduced by an accompanying editorial (16). The typical heart rate of rabbits ranging from 90 to 170 bpm under anesthesia is close to that of the patient in rest and stress cMRI. With proper choice of imaging parameters, most cMRI techniques for humans can be adopted in rabbits without modification. Using ECG triggering and ventilator-assisted respiration holding, the MI size could be quantified by DE-cMRI and these data were found with excellent correlations to the classical histochemical data of infarcted area and volumes (*Figure 2*). We also quantified the global and regional LV functions to confirm, in addition to the characteristic ECG outcomes, the successful MI models in rabbits. Using the integrated Argus software (Siemens), the LV wall thickening could be quantified as color mapped Bull Eyes. The hypokinesis of lateral wall motion can be demonstrated in the MI model as compared to the normal rabbit (*Figure 3*).

To simplify the cMRI operation, we tried to scan

rabbit models of MI without breath holding at a 3.0 T scanner under gas anesthesia and respiration gating (31). Although the absence of breath holding and the presence of respiration gating greatly increased TR, the endotracheal intubation procedure could thus be avoided. This modification more closely simulated clinical conditions, ensured animal safety during the respiration gating cMRI acquisition, and enabled prolonged perfusion weighted cMRI, which otherwise would be impossible by one breath holding (18). The imaging resolution at 3.0 T without breath holding appeared almost the same as that at 1.5 T with breath holding (*Figure 2*), yielding results similar to that with clinic patients (32,33).

Finding LM in rabbits with chronic MI

So far most of the animal experiments on IHD have focused on acute or subacute MI over hours and days, but the follow-up by cMRI over months have not been found in the literature. To investigate the fate of the animals with MI, we observed a few rabbits with MI during acute (days), subacute (weeks) and chronic (months) phases by serial cMRI monitoring and encountered a surprising phenomenon as narrated below.

Heart lipomatosis denotes a variable degree of fat deposition in-between or in some instances in place of the cardiac myocytes (34), which is an uncommon clinical condition in humans and animals. Whereas LM, a pathological alteration secondary to hypoxia, ischemia and infarction with undetermined mechanisms, has been increasingly reported by clinical studies (35), rarely mentioned in veterinary literature (36), and so far not yet established both *in vivo* and *ex vivo* by animal experiments.

Up to now, fatty infiltration of the heart has been reported in a single case of dog with atrial adipofibrosis (37) and one case of cat with generalized fatty infiltration of both atria and ventricles (36). In our research on rabbit models studied by cMRI, we incidentally identified the LM in three rabbits with various extents of healed MI during a 9-month longitudinal follow-up. We revealed the transformation from acute MI to the scar and the transmural deposition of fatty tissue by using cMRI at a 3.0 T clinic magnet, compared *in vivo* cMRI outcomes with postmortem findings, and confirmed the presence of LM as a particular pathology by histochemistry (31). To the best of our knowledge from current literature, this is the first report that fat infiltration involving the left ventricle has been described in experimental animals with chronic

Table 1 Overview of parameters from cMRI studies on rabbit models of ischemic heart disease

Type	Tesla	Coil; channel	Rabbit model	Sequences	Assessment	Res. control	Corresponding sequences parameters					
							Matrix	Spatial resolution [mm]	Slice thickness [mm]	TR/TE [ms]	Bandwidth [Hz/pixel]	Flip angle [°]
Trio Siemens [Feng 2013]	3.0T	Knee coil; 8-channel	Acute and chronic reper-fused MI	TSE True-FISP (Cine); IR-turbo-FLASH (DE)	Anatomy Function; Infarct tissue	No	240x195	0.9x0.9	3.0	621-2,150/ 15-75	235-305	180
Trio Siemens [Hu 2012; 2010]	3.0T	Dual custom built sad-dle-shaped coils	Chronic MI	Spoiled GE k-space segmented sequence (Cine) phase-sensitive-IR scanning sequences (DE)	Anatomy Function Infarct tissue	Yes	192x154	1.0x0.8	2.5	80.5/3.29 57.4/3.54	NA NA	12 12
Sonata, Siemens [Barkhausen 2002]	1.5T	A single-loop surface coil	Acute MI and chronic MI	IR-turbo-FLASH (DE)	Infarct tissue	Yes	153x256	0.7x0.7	3.0	300/NA	NA	NA
Sonata, Siemens [Feng 2009]	1.5T	knee coil; 8-channel	Acute reperfusion MI	True-FISP (cine) IR-turbo-FLASH (DE)	Function Infarct tissue	Yes	222x384	1.2x0.8	3.0	56.4/1.88 500/1.92	977 360	65 10
Sonata, Siemens [Calcagno 2010]	1.5T	knee coil; 8-channel	Atherosclerotic	TSE Double inversion recovery TSE sequence (DE)	Anatomy Aortic plaques	No	256x256	NA	3.0	800-2,000/ 5.6- 39	NA NA	NA 16
Sonata, Siemens [Mansencal 2010]	1.5T	Cardiac phased-array coil	Actue MI	SSFP (Cine) cross-registered inversion-recovery 2D fast gradient-echo (DE)	Function Infarct tissue	Yes	256x160	0.7x1.0	3.0	2.6/1.6 3.1/1.6	NA NA	45 20

MI, myocardial infarction; Res, respiration; DE, delayed-enhancement; TSE, turbo spin echo; True-FISP, true fast imaging with steady-state precession; SSFP, steady state free precession; IR-turbo-FLASH, inversion recovery turbo fast low angle shot; TR, Repetition time; TE, echo time; cMRI, cardiac magnetic resonance imaging.

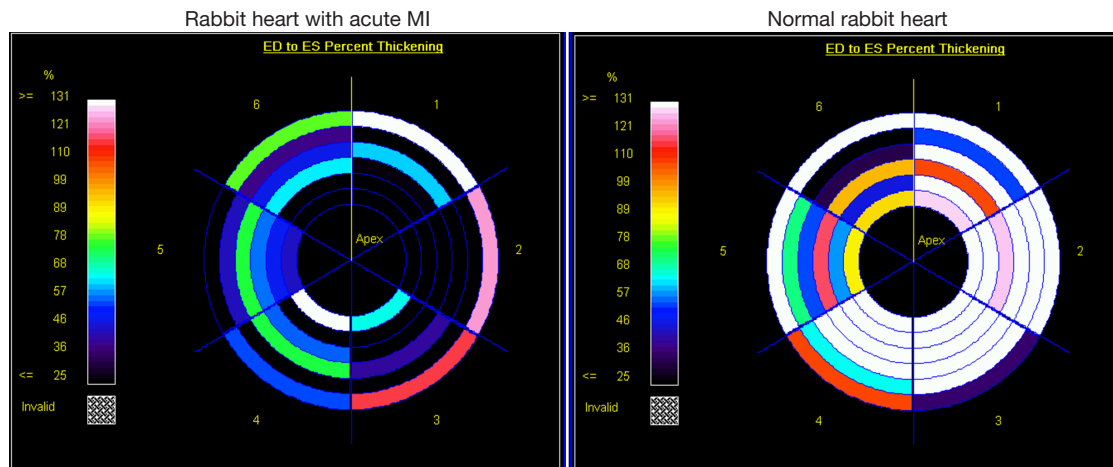


Figure 3 The percent thickening bull-eyes expression for the left ventricles of one rabbit (weight, 3.3 kg; heart rate, 97 bpm) with acute MI on the left and one normal rabbit (weight, 3.3 kg; heart rate, 125 bpm) and the right. MI, myocardial infarction.

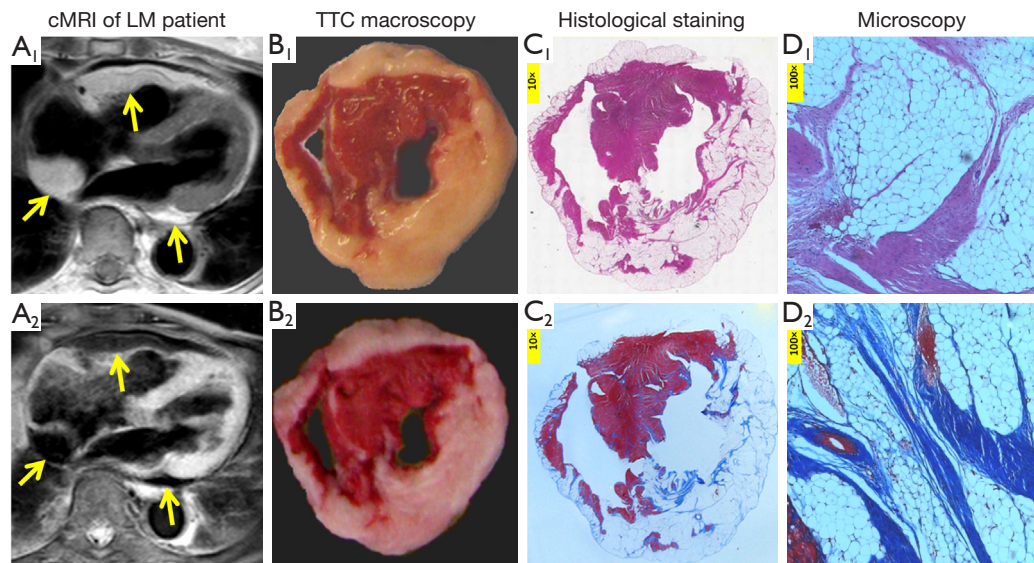


Figure 4 cMRI findings from a human patient with lipomatous metaplasia (LM) and histomorphological findings from a rabbit with LM evolved from chronic MI. (A₁) fast spin echo T1WI without fat suppression reveals the hyperintense LM involving the atrial septum as well as the RV free/lateral wall (arrows); (A₂) fast spin echo T1WI with fat suppression turns the LM spots into hypointense lesions (arrows); (B₁ and B₂) TTC stained heart sections before and 24 h after 10% formalin fixation exhibit a “white MI” from a rabbit (weight, 4.5 kg; heart rate, 167 bpm) with cardiac ischemia for 9 months (formalin fixation helped color differentiation); (C₁ and C₂) HE and MTC stained whole heart sections expose the nature of this “white MI” as LM alteration; (D₁ and D₂) microscopies ($\times 200$) of HE and MTC stained sections prove the presence of collagen scar with abundant adipose cells, confirming the diagnosis of LM in rabbits. cMRI, cardiac magnetic resonance imaging; MI, myocardial infarction; T1WI, T1 weighted imaging; TTC, triphenyltetrazolium chloride; HE, hematoxylin-eosin; MTC, Masson’s trichrome.

MI (31). In *Figure 4*, we first show cMRI manifestations of typical LM from a clinical patient, which simulate the rabbit findings (31) but lack authentic histological proof of its own due to apparent clinical constrains. To compensate

this deficiency we further display the histomorphological sections stained with hematoxylin-eosin (HE) and Masson’s trichrome (MTC) dyes from a rabbit case of LM. By visual inspection, the MI was almost completely replaced

Table 2 Morphometric quantification of cMRI and histology in rabbits with myocardial infarction

Case	Hyperenhanced zone/LV (%) on DE-cMRI			LM after 9M MI on histology		
	24 hours	2 months	9 months	LM/LV % (TTC)	LM/Scar % (HE)	CF/Scar % (MTC)
No.1	42.07	38.25	–	36.94	86.78	13.22
No.2	25.26	17.85	–	16.24	57.88	42.12
No.3	20.55	13.12	–	11.32	55.14	44.86

–, No enhanced region; LM, Lipomatous metaplasia; LV, left ventricle; 9M, 9 month; MI, myocardial infarction; DE-cMRI, contrast delayed enhancement cardiac magnetic resonance imaging; TTC, triphenyltetrazolium chloride staining; HE, hematoxylin-eosin staining; MTC, masson's trichrome staining; CF, collagen fibers.

by LM with a clearly discernable interface against normal myocardium, leading to a phenomenon of “white MI” on heart specimens (*Figure 4*). The involved LV wall was not as atrophied as expected but contralateral normal wall was thickened likely by compensation. The photomicrographs demonstrated high densities of the adipose cells surrounded by few collagen fibers in the LM lesion (*Figure 4*). Microscopically, to quantify the percentage of fat cells in the total scar area, heart sections were scanned with an Axiovert 200 M microscope and captured with a Zeiss AxioCam digital camera using AxioVision 4.7 software. In 10 randomly selected high-power fields over the MI lesion, fat infiltration rate was expressed as the percentage of fat cells divided by total number of cells. As exemplified here, another advantage of using rabbits for this study is the fact that an entire transverse section of the heart can be mounted perfectly on ordinary slide for quantitative microscopic analysis.

Consequently, among three rabbits with chronic MI, morphometric parameters derived from longitudinal cMRI and postmortem analyses are compared in *Table 2*. The MI could be visualized as a hyperenhanced region on DE-cMRI from acute to chronic phase until 2 months but not any longer till 9 months due to vanishing blood vessels in the scar tissue of the late chronic MI. At autopsy, the MI scar over the whole LV varied depending on the initial MI size, whereas at least 50% of the total MI scar was occupied by LM tissue as verified by different histological stainings (*Figure 4*).

Regarding the possible mechanisms for the fatty infiltration in the infarcted myocardium, Pantanowitz *et al.* attributed this pathological alteration to the chronic hypoxia (38). Under hypoxic conditions, fatty acid oxidation decreases, and when intracellular lipids are no longer metabolized by mitochondria, they are extruded and phagocytosed by scar tissues (38). Fatty tissue infiltration in all susceptible species can cause electrical instability,

resulting in life-threatening supraventricular and ventricular arrhythmias, and in some instances valvular dysfunction (38). Additionally, the fatty tissue can induce myocardial toxicity due to the release of certain free fatty acids that can induce arrhythmias and a process known as cardiomyopathy of obesity (39). However, the therapeutic management of adiposity development within scar tissue has been hardly addressed most likely due to a lack of proper animal models. Therefore, the introduced rabbit models of chronic MI can also be used in research for this purpose. Our study also offers a unique opportunity to observe the natural process of this phenomenon in rabbit models that can widen our understanding of related pathophysiology, diagnostics and therapeutics, particularly regenerative medicine after MI.

Imaging MI in rabbits using a necrosis-avid tracer agent

To definitely visualize and quantify MI, a necrosis-specific imaging marker is needed. The current alternative is to detect the MI by using nonspecific extracellular gadolinium contrast agents such as Gd-DTPA and Gd-DOTA, with which the extent and duration of hyperenhanced MI are however multifactorial with potential uncertainties (40,41).

Our research group has a track record in developing novel MRI contrast agents, in particular porphyrin and nonporphyrin necrosis avid contrast agents (NACAs) (40,41). Porphyrins and derivatives have initially been investigated as tumor-localizing agents for cancer optical detection and photodynamic therapy (42,43). By analogy, paramagnetic metalloporphyrins and their analogues have been developed as “tumor-seeking” MRI contrast agents (44,45). However, since the mid 1990s, the previously reported “tumor specificity” of porphyrin analogues has been redefined to be “necrosis avidity” through a series of delicate experimental studies (46,47). These studies not

only converted the real targets of porphyrin-like agents from viable tumor cells to nonviable tissues, but also elicited novel applications for accurate MRI visualization of spontaneous and therapeutic necroses such as acute MI (48-50). Meanwhile, nonporphyrin NACAs that are devoid of discoloration and phototoxicity, the side effects seen with porphyrin species, have been developed and further refined (40,41,51).

Gadophrin-3 as one of the porphyrin-derived NACAs was applied by Barkhausen *et al.* in rabbit models of acute occlusive MI (24). By using this NACA, the authors demonstrated a persistent specific hyperenhancement of the MI in rabbits, which is in line with earlier findings in small and large animals (52-54). However, their major conclusions appeared invalid due to some simple yet fatal defects in their study design. First, the small dose of Gd-DTPA at 0.1 mmol/kg was injected 24 h after a normal dose of Gadophrin-3 that had already assured a striking and persistent hyperenhancement of the MI, which made it impossible for them to separately quantify the enhancement caused by Gadophrin-3 or Gd-DTPA. Instead, they concluded that Gd-DTPA did not overestimate the acute MI size (24). Secondly, it is proven that Gd-DTPA-enhanced area in acute MI can be changeable with time (54) and a delay of 5 to 10 min after Gd-DTPA injection as applied (24) was inadequate for CE-cMRI. In addition, the authors did not perform early phase cMRI after Gadophrin-3 injection, but concluded that chronic MIs do not enhance with Gadophrin-3 (24). Therefore, there still exist rooms for further investigation of NACAs using rabbit models of MI.

After exhausting the last stored non-porphyrin NACAs in our recent rat study (55), due to human reasons beyond the authors' control, such agents have become momentarily unavailable for the current cMRI studies in rabbits. We therefore alternatively studied a novel radioactive infarct-avid tracer agent using a clinical SPECT/CT scanner in the same rabbit models of reperfused MI (27,56).

Non-invasive localization of acute MI and assessment of MI size with an infarct avid agent are deemed essential for estimating the severity, formulating therapeutic strategy, and predicting prognosis in clinical management of IHD. Up to now, infarct avid scintigraphy has not been widely accepted because no such tracers fulfill all required criteria: rapid localization at the infarct, high avidity and specificity, and reasonable duration of scan positivity. In addition, the proper animal models for cardiac scintigraphy are needed for preliminary evaluation and characterization of the necrosis-avid tracers.

Hypericin (Hyp) is a polyphenolic polycyclic quinone originally found in St. John's wort (*Hypericum perforatum*). It is a powerful naturally occurring photosensitizer used in photodynamic therapy in addition to its anti-depressant and antiviral utilities (57). Hyp has recently been recognized as one of the nonporphyrin necrosis avid agents with exceptional necrosis affinity (40,58). In our pursuit for infarct avid tracer agents with optimal properties, we found in preliminary experiments that ^{123}I -Hyp as a radioiodinated Hyp derivative localized in necrotic tissue in rat models of reperfused hepatic infarction (59). The rabbit model of MI was applied in an early study on ^{123}I -Hyp as reported in 2006, which showed the necrosis avidity on MI both *in vivo* and *ex vivo* (58). However, the occlusive MI model there was less clinically relevant, and the number of animals was limited and clinic SPECT modality was not modified (58). Later on, we made some modifications on rabbit models (9), and applied a single pinhole collimator on a dual-head gamma camera to improve the imaging resolution of SPECT images (60). In that study, the potential of ^{123}I -Hyp SPECT in diagnosis of acute MI using rabbit models of myocardial ischemia and occlusive and reperfused MI (60). We compared infarct size estimated with three techniques: *in vivo* ^{123}I -Hyp μSPECT , [^{13}N]ammonia and μPET (60). The major limitation of that study was that the *in vivo* scintigraphic images failed to be matched slice-by-slice with *ex vivo* autoradiographic images and histopathology (60).

In clinical practice, with little redistribution after initial myocardial uptake, $^{99\text{m}}\text{Tc}$ -sestamibi ($^{99\text{m}}\text{Tc}$ -MIBI) has gained widespread use as a perfusion tracer in the evaluation of myocardial viability on SPECT. However, as a new hot-spot tracer, ^{123}I -Hyp has never been compared with $^{99\text{m}}\text{Tc}$ -MIBI for their SPECT capacities. To further validate the necrosis avid tracer ^{123}I -Hyp mediated hot-spot imaging on acute MI, more recently, we explored dual-isotope simultaneous acquisition (DISA)-SPECT/CT by using ^{123}I -Hyp and standard $^{99\text{m}}\text{Tc}$ -MIBI, in comparison with cMRI, autoradiography (AutoRx) and histomorphometry (27). In this study we successfully performed DISA-SPECT/CT using two complementary tracers, ^{123}I -Hyp and $^{99\text{m}}\text{Tc}$ -MIBI to specifically visualize necrotic and normal myocardium respectively, to diagnose the MI. As demonstrated on *Figure 5*, the excellent correspondence between areas of perfusion defect and high ^{123}I -Hyp uptake was depicted from apex to basal, anterior to posterior, and septal to lateral walls. The unique feature of DISA-SPECT/CT permitted to obtain the two independent tracer evaluations during the same session, thus avoiding the variability in

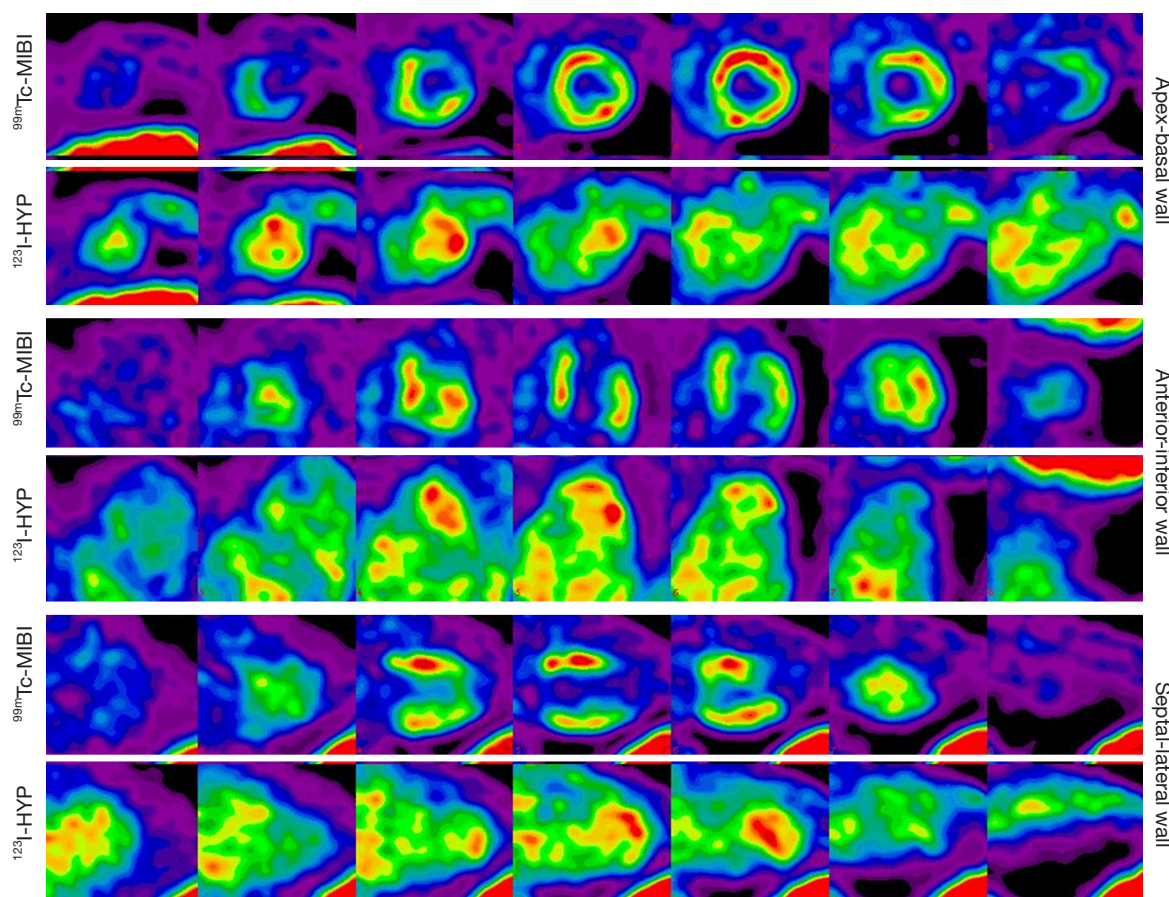


Figure 5 Multi-slice three-orientation views of dual-isotope simultaneous acquisition single photon emission computed tomography (DISA-SPECT) images from a rabbit with acute MI located mainly in the apex. The perfusion tracer ^{99m}Tc -MIBI marked normal LV wall as hyper-radioactive zones (upper rows) leaving the MI as defects. On the contrary, the necrosis-avid tracer ^{123}I -Hyp turned the MI as hot spots with minimum activity found in normal myocardium (lower rows). Therefore, the two tracers are complementary in terms of myocardial viability determination. MI, myocardial infarction.

cardiac anatomy localization due to the possible changes in wall motion (27). Compared to ^{99m}Tc -MIBI, the infarct-avid ^{123}I -Hyp has a longer plasma half-life over 2.5 h, which makes it possible to administer the tracer at ease after the acute cardiac event (60).

We performed the quantification of regional tracers and contrast agent distribution using 17-segment polar maps of the myocardium after co-registration of cMRI, cardiac ^{123}I -Hyp SPECT/CT and ^{99m}Tc -MIBI SPECT/CT images (Figure 6). For MI size quantification based on imaging contrast, a standard threshold adaptable to all individual cases appeared difficult to define due to multiple factors such as lesion size and location, the dosage of, or timing after, tracer/contrast administrations, and with or without reperfusion. However, we were able to adopt co-registered 17-segment

polar maps for semi-quantification and comparison of the MI volumes derived from different imaging modalities (Figure 6). This computer-assisted method standardized the analyses by projecting the 3D information from a complex volume onto a plane. The global and regional LV volumes were automatically calculated and the lesional areas on the 17 segments were manually defined using a five-point scale by three experienced co-workers in consensus. The final MI volumes thus generated could be matched accurately in-between *in vivo* images and verified by postmortem standard references, suggesting that this semi-quantitative method could serve as a viable alternative to the thresholding methods for the MI evaluation (27).

The rabbit model with an entire transverse section of the heart can be perfectly mounted on an ordinary slide for

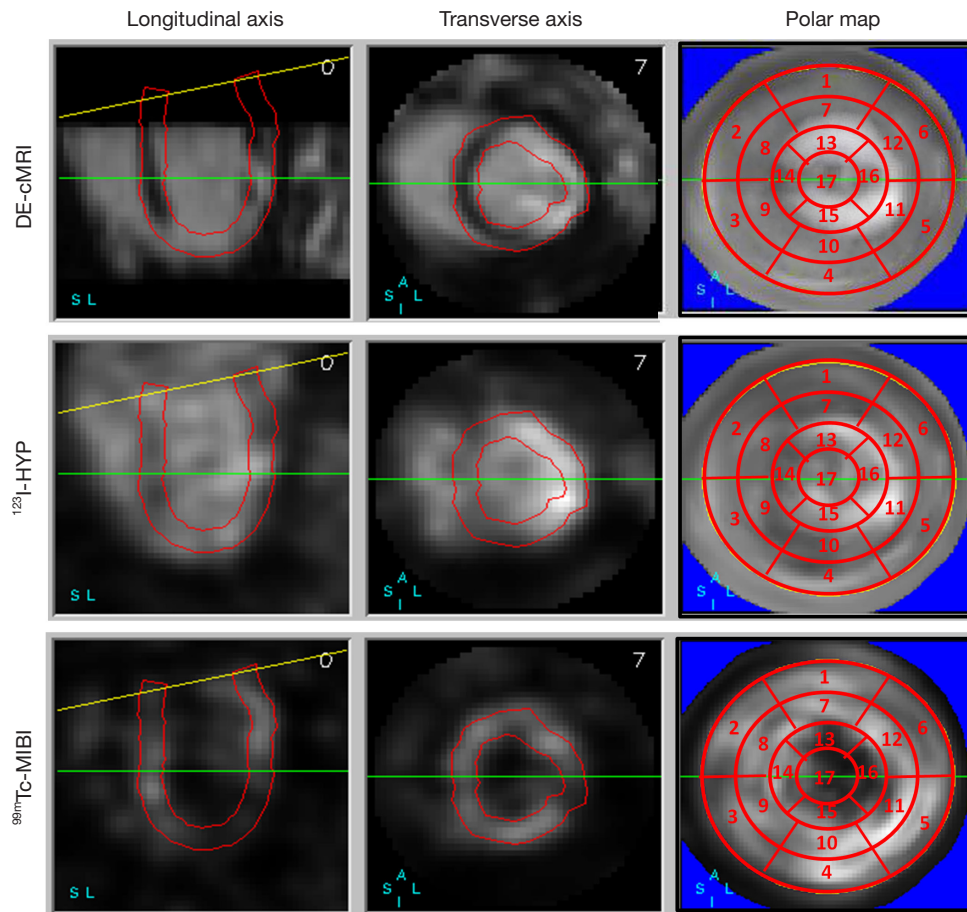


Figure 6 Comparative longitudinal (first column), transverse (second column) axes and polar map (third column) projection and quantification of DE-cMRI and DISA-SPECT with two tracers from the same rabbit of *Figure 5*. Gd-DOTA (first row) and ¹²³I-Hyp (second row) accumulated in the apex-lateral MI, whereas ^{99m}Tc-MIBI (third row) distributed in the rest normal LV wall. Assisted by the dedicated software, 17-segment on polar maps are demonstrated for co-registered MI volume and regional contrast/tracer uptake evaluation. The percentage MI volumes can thus be generated for different imaging modalities. Yellow and green lines used for imaging localization and co-registration. DISA-SPECT, dual-isotope simultaneous acquisition-single photon emission computer tomography; MI, myocardial infarction; LV, left ventricular.

microscopy. This feature has made it more convenient to quantify radioactivity by autoradiography for necrotic and normal tissues and to view the highly fluorescent ¹²³I-Hyp in acute MI in contrast to the low fluorescence in viable myocardium over the entire LV (56).

Despite a great diversity in chemical structures and physicochemical properties among the various necrosis-avid tracer agents for nuclear medicine and NACAs for MRI, common physicochemical interactions could be shared by at least some of these agents. The meticulous and accurate methodologies applied on the rabbit models allow us to carefully analyze the relationship between structure and uptake/retention of the known necrosis-avid agents in

necrotic tissue. This may provide deeper insights into the mechanisms of this unique phenomenon and yield useful information regarding the structural requirements for further optimization of this type of agents.

Stratifying acute MI components in rabbits using multifunctional images

The myocardial area at risk (AAR) is defined as the myocardial tissue within the perfusion bed that is distal to the culprit lesion of the infarct-related CA. Since the AAR includes both damaged nonviable MI-core and viable or salvageable zone (SZ), the proportion of SZ within

the AAR depends on multiple factors including time to reperfusion, ischemic pre-conditioning, collateral flow, distal embolization, reperfusion injury, and microvascular dysfunction. Because the extent of SZ determines final infarct size, quantifications of MI components provide an accurate index in clinical practice and preclinical research for diagnostic, therapeutic and prognostic assessment of the IHD.

Myocardial AAR research on ischemic injury has been demonstrated in a wide variety of animal models of acute myocardial ischemia-reperfusion, including large species such as swine and smaller rodents such as rats (61,62), but before our endeavors it had not been reported in rabbit hearts by means of combined *in vivo* and *ex vivo* imaging studies.

Quantification of the AAR proved challenging both *in vivo* and *ex vivo*. Radiolabeled or fluorescent microspheres are the reference standard for measuring the AAR in animal studies without information of whole heart topography (62). Usually, Evans blue (EB) dye was retrograde injected during re-occlusion of the CA branch to visualize the AAR postmortem in most studies (63,64). However, radiolabeled microspheres impose potential hazard for radiation exposure, while colored microspheres require tissue lysis for counting, with both lacking morphometric information. Besides, water-soluble EB dye has recently been found with necrosis affinity (65), thus unsuitable for infarct-normal myocardial delineation.

In humans, the most widely used technique is SPECT, but many drawbacks such as poor spatial and temporal resolutions prevent its widespread use. Cardiac MRI however could be an attractive technique to noninvasively quantify the AAR by several methods, which though still remain controversies (66,67).

Given the above-specified problems, we attempted in our rabbit models to accurately evaluate three major myocardial ischemic components, namely the AAR, MI-core and SZ, known to be the key elements in clinical and experimental cardiology. The methods we have developed were technically different from those previously described by others and are summarized here. First, during the open-chest operation, two sutures, instead of one, were placed underneath the CA branch sharing the same stitch, one for the CA occlusion and reperfusion *in vivo* and the other for postmortem CA re-occlusion before coronary angiography. Secondly, perfusion weighted imaging (PWI) was acquired pre and post CA reperfusion separately before and after pulling the exteriorized end of ligation suture. Third, EB solution as a necrosis marker was intravenously

injected hours after CA reperfusion to visualize the MI-core postmortem. Fourth, a bifunctional dye for *ex vivo* determination of the AAR was invented and successfully applied in rabbit studies (17,18).

The technical hints of this multifunctional staining method are given below. After cMRI, heparin was intravenously administered to prevent blood coagulation. The heart was excised under deep anesthesia, a plastic catheter was inserted into the aorta, and the coronary bed was rinsed with normal saline. Following CA re-ligation with the prior spared 5-0 suture, the newly invented red iodized oil (RIO) was infused, in conjunction with the *in vivo* injected EB dye, for multiple stainings of the AAR, SZ and MI-core and postmortem myocardial digital radiography (DR) (17,18). *Figure 7* demonstrates a rabbit with massive reperfused MI. A complete series of six transverse sections of the infarcted heart could be visualized by *in vivo* DE-cMRI and *ex vivo* DR and multifunctional staining techniques combining the two dyes of EB and RIO. The MI-core was already stained dark blue by the intravital necrosis avid dye EB. The AAR was clearly shown as a nonopacified region on DR and oil-red-O unstained region by RIO. The SZ appeared whitish in-between the blue-stained MI-core and red-stained normal heart. Since this case had a huge haemorrhagic MI after 90-min CA occlusion and 24 h CA reperfusion, the SZ was relatively small and the cardiac apex became almost entirely necrotic. This way, the real AAR, MI-core and SZ could be simultaneously visualized, located and delineated for further quantitative analyses (17,18). Such an *ex vivo* method can already be applied in translational theragnostic cardiology for pathophysiological studies or drug development, but the real *in vivo* applications among clinical patients of IHD still rely on the availability of NACAs for absolute determination of MI-core (40,41).

To further validate the high necrotic avidity of EB dye for labeling necrotic myocardium in addition to necrosis in tumors (55) and other organs (65), we correlated *in vivo* and *ex vivo* cMRI, fluorescent and histological findings in rabbits with acute reperfused MI as shown in *Figure 8*. The MI on the left anteriolateral LV wall could be hyperenhanced on DE-cMRI (*Figure 8A*) and *ex vivo* T1 MRI (*Figure 8B*), however the MI lesion appeared hypointense on *ex vivo* T2 MRI due to hemorrhage in this reperfused MI (*Figure 8C*). The intravenously injected EB dye could specifically stain only the irreversible necrotic myocardium as a dark blue region, but the viable myocardium even surrounded by necrosis remained not blue-stained (*Figure 8D*). EB

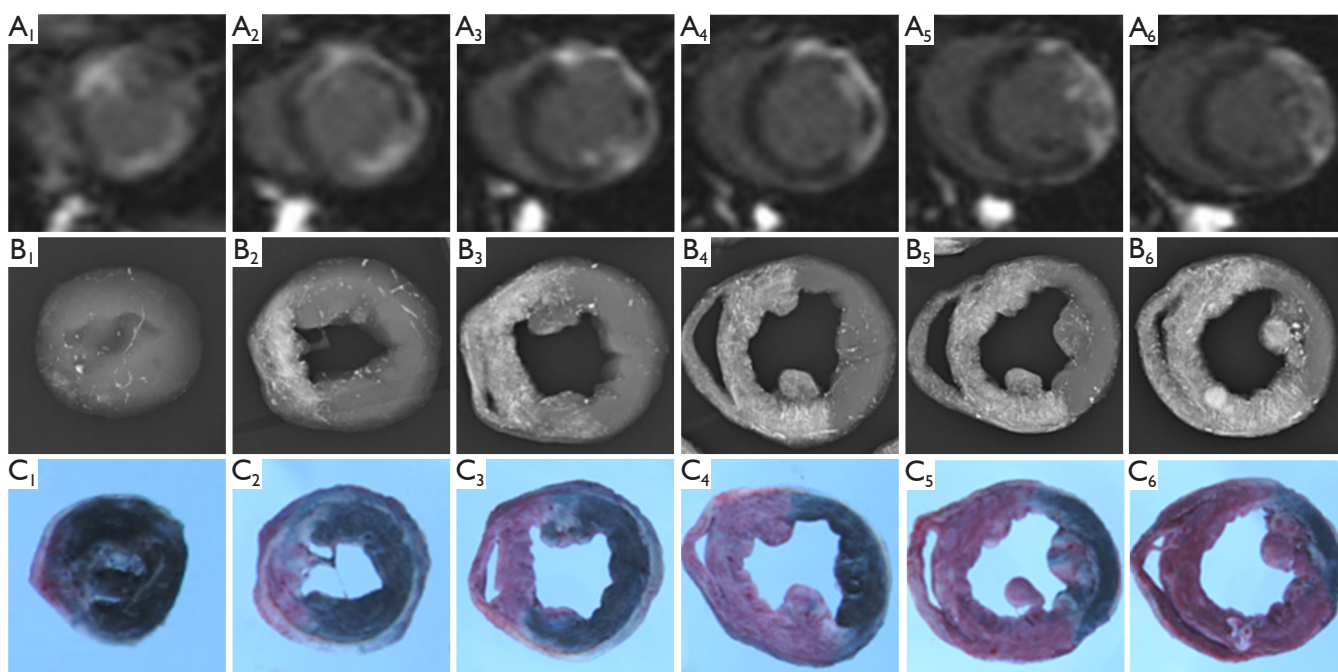


Figure 7 DE-cMRI, digital radiography (DR) and multifunctional staining images from a rabbit with massive acute reperfused MI. (A₁₋₆) Serial DE-cMRI images from the apex to base reveal a hyperenhanced MI, wherein the heterogeneity was due to hemorrhage; (B₁₋₆) serial DR images from the apex to base demonstrate a perfusion defect of this massive MI, corresponding to the *in vivo* cMRI findings (A₁₋₆); (C₁₋₆) serial multifunctional staining images stratify the tissue components of the MI: the RIO dye stained red region represents the normal well perfused myocardium and the rest correspond to the area at risk (AAR); the EB stained dark blue zone indicates the irreversible necrotic MI-core in this massive reperfused and hemorrhagic MI; and the scattered unstained whitish areas at the infarct periphery refer to the ischemic but salvageable zone (SZ). Thus, the AAR included both the MI-core and SZ. The SZ could be larger if the coronary artery was occluded shorter than 90 minutes in this case. MI, myocardial infarction; cMRI, cardiac magnetic resonance imaging; DE, delayed enhanced; RIO, red iodized oil; EB, Evans blue.

dye showed also strong red-fluorescence in its stained MI under fluorescent microscopy (Figure 8E) and the presence of MI could be confirmed by histology by HE staining (Figure 8F). Interestingly, although both Hyp and EB are necrosis-avid compounds (41), Hyp emits red-fluorescence from necroses both macro- and microscopically, but EB could show only microscopic red-fluorescence. The reason for such a difference has to be elucidated. This result further confirmed high necrosis-avidity of EB dye, suggesting a novel application in experimental cardiology.

For *in vivo* evaluations of the AAR and myocardial salvageable index using cMRI, we successfully performed first-pass PWI on rabbit models of MI (18). To our knowledge, it is the first report of PWI in rabbits. Comparing with conventional T2WI, we found that quantification of the AAR by PWI acquired at the condition of CA occlusion appeared closest to the standard reference with multifunctional staining techniques. This finding is in

favor of the opinion that T2WI overestimates the AAR in acute MI (67). Therefore, the present experimental platform based on rabbit models and multimodal imaging techniques proves useful for *in vivo* and *ex vivo* stratification of ischemic components particularly the AAR research.

Assessing new therapeutics for the treatment of acute MI in rabbits

Among the cardiovascular pathologies, IHD is the leading cause of congestive heart failure as well as permanent premature disabilities. Reperfusion of a previously ischemic heart is a standard clinical therapeutic procedure. Even if beneficial, reperfusion triggers inflammatory responses that contribute to the acute extension of ischemic injury and later participate in the reparative processes of the damaged myocardium. Occlusion of a major CA in animal model, followed or not followed by reperfusion, has proven to be a

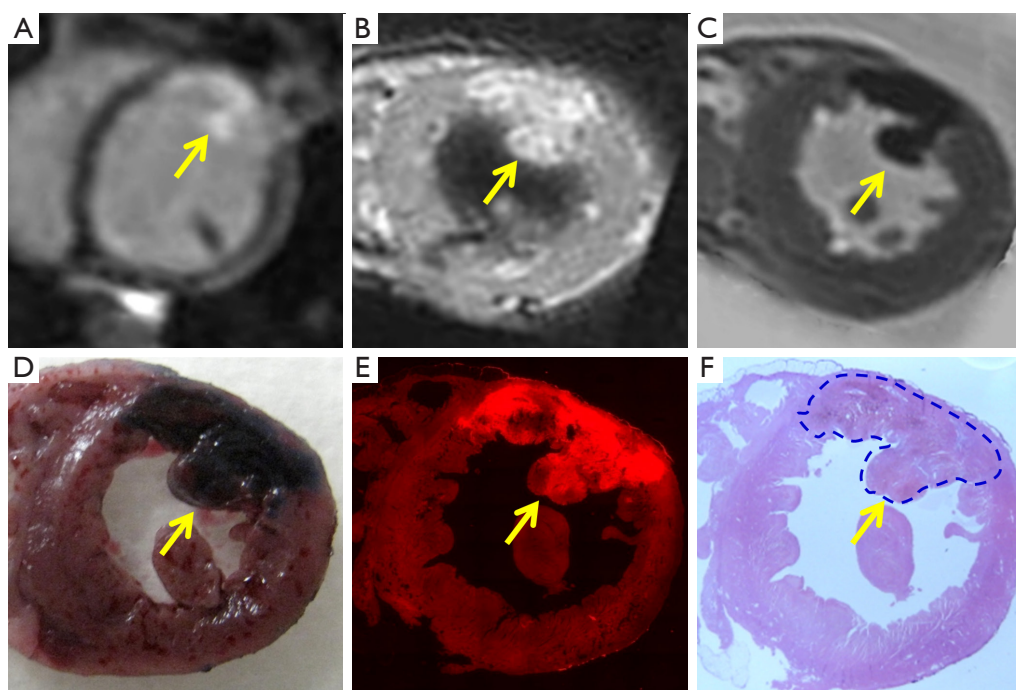


Figure 8 *In vivo* and *ex vivo* cMRI and intravital EB staining outcomes from a rabbit with acute MI. (A) *In vivo* DE-cMRI displays a hyperenhanced transmurular MI (arrow) involving the anterior papillary muscle; (B) *ex vivo* DE-cMRI shows the same MI (arrow) with higher spatial and contrast resolutions; (C) *ex vivo* T2W-cMRI reveals this MI as a hypointense lesion (arrow) because of the hemorrhage after reperfusion; (D) fresh cardiac section presents the MI as an EB stained dark blue region (arrow); (E) fluorescence microscopy ($\times 10$) turns the MI into a bright red lesion, proving the fluorescent property of the necrotic EB dye. Comparing the details from D and E, the EB-unstained spots are also not fluorescent, suggesting the specificity of this intravital dye; (F) H-E stained microscopy ($\times 10$) confirms the presence of this transmurular MI (arrow). cMRI, cardiac magnetic resonance imaging; EB, Evans blue; DE, delayed enhanced; MI, myocardial infarction; HE, hematoxylin-eosin.

good approach to assess the relevance of pathophysiological processes and drug effects in the setting of myocardial ischemia (64,68). Models involving reperfusion appear to be particularly suitable to study the inflammatory response and therefore much more clinically relevant than that with permanent ischemia. Animal models of myocardial ischemia/reperfusion allow the possibility of testing a vast array of molecular mediators that orchestrate the sequelae of inflammation, and such models also allow testing of the protective effects of anti-inflammatory drugs in experimental MI.

Rodents are the most popular laboratory animals in cardiovascular therapeutic research, since the knockout and transgenic models have been instrumental in understanding the molecular and cellular mechanisms in the IHD and in comparing the effects of existing and new anti-inflammation or anti ischemia-reperfusion injury drugs (5,9,69), just as they have been comprehensively applied in the basic molecular, cellular and cardiovascular biology (20,70). However, significant differences do exist with regard to

several cardiac characteristics when rodents are compared with humans. Besides, the small cardiac dimension and high heart beating rate limit the use of cardiac imaging modalities for *in vivo* therapeutic evaluations. For these reasons, large animal models including dogs, sheep and pigs have been established and applied in cardiac research. Although they can mimic human patients to a broad extent and can create experimental data pertinent to the scenarios for the diagnosis and differential diagnosis as well as therapeutic regimes in clinical cardiology, the high expenses, demanding housing conditions and tough handling would constrain their wide applications (9).

To validate whether the rabbit models of MI and the imaging-based technique platform that we have developed are suitable for the research on medicinal intervention of acute MI, we conducted preliminary experiments on cannabidiol (CBD) for its potential in the treatment of MI (71). CBD, a major nonpsychoactive and noncognitive constituent of the plant *Cannabis sativa*, has been

found with multiple pharmacological actions including anxiolytic, antipsychotic, antioxidant, anti-inflammatory, immunomodulatory and antiemetic properties (72). A growing line of evidence indicates that CBD has also been associated with beneficial effects in the modulation of physiopathological activities in the cardiovascular system (73). However, up to now, the majority of studies on CBD have been focused on small rodent models (68,74), and CBD has not been investigated in medium or large size animal models.

Combining *in vivo* cMRI and multiple postmortem techniques by using our imaging-based theragnostic platform and rabbit models of acute MI, we have been able to report that two times of CBD administration (100 µg/kg) at 10 min before LCx occlusion and 10 min prior to LCx reperfusion exerted cardioprotective effects in rabbit models of acute ischemia-reperfusion injury (71). In particular, CBD significantly decreased the release of troponin I, which is cardiac damage specific biomarkers in the blood, reduced infarct size (AMI-core/AAR) and improved myocardial salvageable index (MSI). In addition, CBD increased relative blood flow in the AAR and thus reserved more regional cardiac functions as demonstrated by *in vivo* cMRI and confirmed by *ex vivo* multifunctional staining. Such protection from reperfusion injury was most likely associated with reduced infiltrating neutrophils and myeloperoxidase activity as shown histochemically (71).

Thus, we successfully evaluated the therapeutic potency of CBD as a natural compound in rabbit models of myocardial ischemia/reperfusion injury based on our pre-established methodology and technical platform.

Conclusions

Ongoing cardiologic research on pathologies of IHD and other related cardiac disorders in translational medicine has benefited from the developments of improved rabbit models of MI, advanced imaging techniques and novel methods for multifunctional staining of post-ischemic tissue components as overviewed above. This methodology may contribute substantially to developing new diagnostics and therapeutics in translational cardiology.

Acknowledgements

This study was partially supported by the grants awarded by a EU project Asia-Link CfP 2006-EuropeAid/123738/

C/ACT/Multi-Proposal No. 128-498/111, the KU Leuven Molecular Small Animal Imaging Center MoSAIC (KUL EF/05/08) and KU Leuven the center of excellence *In vivo* Molecular Imaging Research (IMIR). The corresponding author Ni Y is currently a Bayer Lecture Chair holder.

Disclosure: The authors declare no conflict of interest.

References

1. Kramer CM, Sinusas AJ, Sosnovik DE, French BA, Bengel FM. Multimodality imaging of myocardial injury and remodeling. *J Nucl Med* 2010;51 Suppl 1:107S-121S.
2. Arai AE. Magnetic resonance imaging for area at risk, myocardial infarction, and myocardial salvage. *J Cardiovasc Pharmacol Ther* 2011;16:313-20.
3. Beller GA, Heede RC. SPECT imaging for detecting coronary artery disease and determining prognosis by noninvasive assessment of myocardial perfusion and myocardial viability. *J Cardiovasc Transl Res* 2011;4:416-24.
4. Krombach GA, Niendorf T, Günther RW, Mahnken AH. Characterization of myocardial viability using MR and CT imaging. *Eur Radiol* 2007;17:1433-44.
5. Epstein FH. MR in mouse models of cardiac disease. *NMR Biomed* 2007;20:238-55.
6. Wang H, Li J, Chen F, De Keyser F, Yu J, Feng Y, Nuyts J, Marchal G, Ni Y. Morphological, functional and metabolic imaging biomarkers: assessment of vascular-disrupting effect on rodent liver tumours. *Eur Radiol* 2010;20:2013-26.
7. Dixon JA, Spinale FG. Large animal models of heart failure: a critical link in the translation of basic science to clinical practice. *Circ Heart Fail* 2009;2:262-71.
8. Nguyen Din Cat A, Sainte-Marie Y, Jaisser F. Animal models in cardiovascular diseases: new insights from conditional models. *Handb Exp Pharmacol* 2007;(178):377-405.
9. Feng Y, Xie Y, Wang H, Chen F, Ye Y, Jin L, Marchal G, Ni Y. A modified rabbit model of reperfused myocardial infarction for cardiac MR imaging research. *Int J Cardiovasc Imaging* 2009;25:289-98.
10. Lin JF, Lin SM, Chih CL, Nien MW, Su HH, Hu BR, Huang SS, Tsai SK. Resveratrol reduces infarct size and improves ventricular function after myocardial ischemia in rats. *Life Sci* 2008;83:313-7.
11. Zbinden G, Bagdon RE. Isoproterenol-induced heart necrosis, an experimental model for the study of angina pectoris and myocardial infarct. *Rev Can Biol*

- 1963;22:257-63.
12. Adler N, Camin LL, Shulkin P. Rat model for acute myocardial infarction: application to technetium-labeled glucoheptonate, tetracycline, and polyphosphate. *J Nucl Med* 1976;17:203-7.
 13. Suzuki Y, Lyons JK, Yeung AC, Ikeno F. In vivo porcine model of reperfused myocardial infarction: in situ double staining to measure precise infarct area/area at risk. *Catheter Cardiovasc Interv* 2008;71:100-7.
 14. Sabbah HN, Stein PD, Kono T, Gheorghide M, Levine TB, Jafri S, Hawkins ET, Goldstein S. A canine model of chronic heart failure produced by multiple sequential coronary microembolizations. *Am J Physiol* 1991;260:H1379-84.
 15. Shiomi M, Yamada S, Matsukawa A, Itabe H, Ito T. Invasion of atheromatous plaques into tunica media causes coronary outward remodeling in WHHLMI rabbits. *Atherosclerosis* 2008;198:287-93.
 16. van der Laarse A, van der Wall EE. Rabbit models: ideal for imaging purposes? *Int J Cardiovasc Imaging* 2009;25:299-301.
 17. Feng Y, Ma Z, Chen F, Yu J, Cona MM, Xie Y, Li Y, Ni Y. Bifunctional staining for ex vivo determination of area at risk in rabbits with reperfused myocardial infarction. *World J Methodol* 2013;3:27-38.
 18. Feng Y, Chen F, Ma Z, Dekeyzer F, Yu J, Xie Y, Cona MM, Oyen R, Ni Y. Towards stratifying ischemic components by cardiac MRI and multifunctional stainings in a rabbit model of myocardial infarction. *Theranostics* 2013;4:24-35.
 19. Lim TH, Choi SI. MRI of myocardial infarction. *J Magn Reson Imaging* 1999;10:686-93.
 20. Grauss RW, van Tuyn J, Steendijk P, Winter EM, Pijnappels DA, Hogers B, Gittenberger-De Groot AC, van der Geest R, van der Laarse A, de Vries AA, Schalij MJ, Atsma DE. Forced myocardin expression enhances the therapeutic effect of human mesenchymal stem cells after transplantation in ischemic mouse hearts. *Stem Cells* 2008;26:1083-93.
 21. Odening KE, Jung BA, Lang CN, Cabrera Lozoya R, Ziupa D, Menza M, Relan J, Franke G, Perez Feliz S, Koren G, Zehender M, Bode C, Brunner M, Sermesant M, Föll D. Spatial correlation of action potential duration and diastolic dysfunction in transgenic and drug-induced LQT2 rabbits. *Heart Rhythm* 2013;10:1533-41.
 22. Calcagno C, Vucic E, Mani V, Goldschlager G, Fayad ZA. Reproducibility of black blood dynamic contrast-enhanced magnetic resonance imaging in aortic plaques of atherosclerotic rabbits. *J Magn Reson Imaging* 2010;32:191-8.
 23. Qi XL, Liu J, Burns PN, Wright GA. The Characteristics of Vascular Growth in VX2 Tumor Measured by MRI and Micro-CT. *J Oncol* 2012;2012:362096.
 24. Barkhausen J, Ebert W, Debatin JF, Weinmann HJ. Imaging of myocardial infarction: comparison of magnevist and gadophrin-3 in rabbits. *J Am Coll Cardiol* 2002;39:1392-8.
 25. Mansencal N, Tissier R, Deux JF, Ghaleh B, Couvreur N, Rienzo M, Guéret P, Rahmouni A, Berdeaux A, Garot J. Relation of the ischaemic substrate to left ventricular remodelling by cardiac magnetic resonance at 1.5 T in rabbits. *Eur Radiol* 2010;20:1214-20.
 26. Saeed M, Weber O, Lee R, Do L, Martin A, Saloner D, Ursell P, Robert P, Corot C, Higgins CB. Discrimination of myocardial acute and chronic (scar) infarctions on delayed contrast enhanced magnetic resonance imaging with intravascular magnetic resonance contrast media. *J Am Coll Cardiol* 2006;48:1961-8.
 27. Feng Y, Cona MM, Vunckx K, Li Y, Chen F, Nuyts J, Gheysens O, Zhou L, Xie Y, Oyen R, Ni Y. Detection and quantification of acute reperfused myocardial infarction in rabbits using DISA-SPECT/CT and 3.0T cardiac MRI. *Int J Cardiol* 2013;168:4191-8.
 28. Hu N, Straub CM, Garzarelli AA, Sabey KH, Yockman JW, Bull DA. Ligation of the left circumflex coronary artery with subsequent MRI and histopathology in rabbits. *J Am Assoc Lab Anim Sci* 2010;49:838-44.
 29. Hu N, Sabey KH, Curtis HR, Hoang N, Dowdle SB, Garzarelli AA, Buswell HR, Dibella E, Yockman JW, Bull DA. Magnetic resonance imaging (MRI) assessment of ventricular remodeling after myocardial infarction in rabbits. *Comp Med* 2012;62:116-23.
 30. Willinek WA, Schild HH. Clinical advantages of 3.0 T MRI over 1.5 T. *Eur J Radiol* 2008;65:2-14.
 31. Feng Y, Chen F, Xie Y, Wang H, Cona MM, Yu J, Li J, Bogaert J, Janssens S, Oyen R, Ni Y. Lipomatous metaplasia identified in rabbits with reperfused myocardial infarction by 3.0 T magnetic resonance imaging and histopathology. *BMC Med Imaging* 2013;13:18.
 32. Greenman RL, Shirosky JE, Mulkern RV, Rofsky NM. Double inversion black-blood fast spin-echo imaging of the human heart: a comparison between 1.5T and 3.0T. *J Magn Reson Imaging* 2003;17:648-55.
 33. Gutberlet M, Spors B, Grothoff M, Freyhardt P, Schwinge K, Plotkin M, Amthauer H, Noeske R, Felix R. Comparison of different cardiac MRI sequences at 1.5

- T/3.0 T with respect to signal-to-noise and contrast-to-noise ratios - initial experience. *Rofo* 2004;176:801-8.
34. Agudelo CF, Svoboda M, Husnik R, Dvir S. Heart lipomatosis in domestic animals: a review. *Vet Med* 2013;58:252-9.
 35. Arnold JR, Karamitsos TD, Pegg TJ, Francis JM, Neubauer S. Left ventricular lipomatous metaplasia following myocardial infarction. *Int J Cardiol* 2009;137:e11-2.
 36. Agudelo CF, Fictum P, Skoric M, Kazbundova K, Svoboda M, Scheer P. Unusual massive fatty infiltration of the heart in a British cat: a case report. *Vet Med* 2011;56:145-7.
 37. Une Y, Furusawa N, Shiota K, Nomura Y. Atrial adipofibrosis in a dog. *J Vet Diagn Invest* 1998;10:192-4.
 38. Pantanowitz L. Fat infiltration in the heart. *Heart* 2001;85:253.
 39. Poirier P, Giles TD, Bray GA, Hong Y, Stern JS, Pi-Sunyer FX, Eckel RH. Obesity and cardiovascular disease: pathophysiology, evaluation, and effect of weight loss. *Arterioscler Thromb Vasc Biol* 2006;26:968-76.
 40. Ni Y, Bormans G, Chen F, Verbruggen A, Marchal G. Necrosis avid contrast agents: functional similarity versus structural diversity. *Invest Radiol* 2005;40:526-35.
 41. Ni Y. Metalloporphyrins and functional analogues as MRI contrast agents. *Curr Med Imaging Rev* 2008;4:96-112.
 42. Gomer CJ. Photodynamic therapy in the treatment of malignancies. *Semin Hematol* 1989;26:27-34.
 43. Pass HI. Photodynamic therapy in oncology: mechanisms and clinical use. *J Natl Cancer Inst* 1993;85:443-56.
 44. Nelson JA, Schmiedl U, Shankland EG. Metalloporphyrins as tumor-seeking MRI contrast media and as potential selective treatment sensitizers. *Invest Radiol* 1990;25 Suppl 1:S71-3.
 45. Fiel RJ, Musser DA, Mark EH, Mazurchuk R, Alletto JJ. A comparative study of manganese meso-sulfonatophenyl porphyrins: contrast-enhancing agents for tumors. *Magn Reson Imaging* 1990;8:255-9.
 46. Ni Y, Marchal G, Yu J, Lukito G, Petré C, Wevers M, Baert AL, Ebert W, Hilger CS, Maier FK. Localization of metalloporphyrin-induced "specific" enhancement in experimental liver tumors: comparison of magnetic resonance imaging, microangiographic, and histologic findings. *Acad Radiol* 1995;2:687-99.
 47. Ni Y, Petré C, Miao Y, Yu J, Cresens E, Adriaens P, Bosmans H, Semmler W, Baert AL, Marchal G. Magnetic resonance imaging-histomorphologic correlation studies on paramagnetic metalloporphyrins in rat models of necrosis. *Invest Radiol* 1997;32:770-9.
 48. Ni Y, Pislaru C, Bosmans H, Pislaru S, Miao Y, Van de Werf F, Semmler W, Marchal G. Validation of intracoronary delivery of metalloporphyrin as an in vivo "histochemical staining" for myocardial infarction with MR imaging. *Acad Radiol* 1998;5 Suppl 1:S37-41; discussion S45-6.
 49. Ni YC, Marchal G, Petré C, Lukito G, Herijgers P, Flameng W, Hilger CS, Ebert W, Maier FK, Semmler W. Metalloporphyrin enhanced magnetic-resonance-imaging of acute myocardial-infarction. *Circulation* 1994;90:I-468.
 50. Ni Y, Marchal G, Herijgers P, Flameng W, Petré C, Ebert W, Hilger CS, Pfefferer D, Semmler W, Baert AL. Paramagnetic metalloporphyrins: from enhancers of malignant tumors to markers of myocardial infarcts. *Acad Radiol* 1996;3 Suppl 2:S395-7.
 51. Ni Y, Cresens E, Adriaens P, Miao Y, Verbeke K, Dymarkowski S, Verbruggen A, Marchal G. Necrosis-avid contrast agents: introducing nonporphyrin species. *Acad Radiol* 2002;9 Suppl 1:S98-101.
 52. Marchal G, Ni Y, Herijgers P, Flameng W, Petré C, Bosmans H, Yu J, Ebert W, Hilger CS, Pfefferer D, Semmler W, Baert AL. Paramagnetic metalloporphyrins: infarct avid contrast agents for diagnosis of acute myocardial infarction by MRI. *Eur Radiol* 1996;6:2-8.
 53. Pislaru SV, Ni Y, Pislaru C, Bosmans H, Miao Y, Bogaert J, Dymarkowski S, Semmler W, Marchal G, Van de Werf FJ. Noninvasive measurements of infarct size after thrombolysis with a necrosis-avid MRI contrast agent. *Circulation* 1999;99:690-6.
 54. Ni Y, Pislaru C, Bosmans H, Pislaru S, Miao Y, Bogaert J, Dymarkowski S, Yu J, Semmler W, Van de Werf F, Baert AL, Marchal G. Intracoronary delivery of Gd-DTPA and Gadophrin-2 for determination of myocardial viability with MR imaging. *Eur Radiol* 2001;11:876-83.
 55. Wang H, Miranda Cona M, Chen F, Li J, Yu J, Feng Y, Peeters R, De Keyzer F, Marchal G, Ni Y. Comparison between nonspecific and necrosis-avid gadolinium contrast agents in vascular disrupting agent-induced necrosis of rodent tumors at 3.0T. *Invest Radiol* 2011;46:531-8.
 56. Cona MM, Feng Y, Li Y, Chen F, Vunckx K, Zhou L, Van Slambrouck K, Rezaei A, Gheysens O, Nuyts J, Verbruggen A, Oyen R, Ni Y. Comparative study of iodine-123-labeled-hypericin and (99m)Tc-labeled hexakis [2-methoxyisobutylisonitril] in a rabbit model of myocardial infarction. *J Cardiovasc Pharmacol* 2013;62:304-11.
 57. Chen B, Zupkó I, de Witte PA. Photodynamic therapy with hypericin in a mouse P388 tumor model: vascular

- effects determine the efficacy. *Int J Oncol* 2001;18:737-42.
58. Ni Y, Huyghe D, Verbeke K, de Witte PA, Nuyts J, Mortelmans L, Chen F, Marchal G, Verbruggen AM, Bormans GM. First preclinical evaluation of mono-[123I] iodohypericin as a necrosis-avid tracer agent. *Eur J Nucl Med Mol Imaging* 2006;33:595-601.
 59. Fonge H, Jin L, Wang H, Ni Y, Bormans G, Verbruggen A. Synthesis and preliminary evaluation of mono-[123I] iodohypericin monocarboxylic acid as a necrosis avid imaging agent. *Bioorg Med Chem Lett* 2007;17:4001-5.
 60. Fonge H, Vunckx K, Wang H, Feng Y, Mortelmans L, Nuyts J, Bormans G, Verbruggen A, Ni Y. Non-invasive detection and quantification of acute myocardial infarction in rabbits using mono-[123I]iodohypericin microSPECT. *Eur Heart J* 2008;29:260-9.
 61. Mewton N, Rapacchi S, Augeul L, Ferrera R, Loufouat J, Bousset L, Micolich A, Rioufol G, Revel D, Ovize M, Croisille P. Determination of the myocardial area at risk with pre- versus post-reperfusion imaging techniques in the pig model. *Basic Res Cardiol* 2011;106:1247-57.
 62. Arheden H, Saeed M, Higgins CB, Gao DW, Ursell PC, Bremerich J, Wytttenbach R, Dae MW, Wendland MF. Reperfused rat myocardium subjected to various durations of ischemia: estimation of the distribution volume of contrast material with echo-planar MR imaging. *Radiology* 2000;215:520-8.
 63. Michael LH, Entman ML, Hartley CJ, Youker KA, Zhu J, Hall SR, Hawkins HK, Berens K, Ballantyne CM. Myocardial ischemia and reperfusion: a murine model. *Am J Physiol* 1995;269:H2147-54.
 64. Liu X, Huang Y, Pokreisz P, Vermeersch P, Marsboom G, Swinnen M, Verbeken E, Santos J, Pellens M, Gillijns H, Van de Werf F, Bloch KD, Janssens S. Nitric oxide inhalation improves microvascular flow and decreases infarction size after myocardial ischemia and reperfusion. *J Am Coll Cardiol* 2007;50:808-17.
 65. Li J, Cona MM, Chen F, Feng Y, Zhou L, Yu J, Nuyts J, de Witte P, Zhang J, Himmelreich U, Verbruggen A, Ni Y. Exploring theranostic potentials of radioiodinated hypericin in rodent necrosis models. *Theranostics* 2012;2:1010-9.
 66. Arai AE, Leung S, Kellman P. Controversies in cardiovascular MR imaging: reasons why imaging myocardial T2 has clinical and pathophysiologic value in acute myocardial infarction. *Radiology* 2012;265:23-32.
 67. Croisille P, Kim HW, Kim RJ. Controversies in cardiovascular MR imaging: T2-weighted imaging should not be used to delineate the area at risk in ischemic myocardial injury. *Radiology* 2012;265:12-22.
 68. Walsh SK, Hepburn CY, Kane KA, Wainwright CL. Acute administration of cannabidiol in vivo suppresses ischaemia-induced cardiac arrhythmias and reduces infarct size when given at reperfusion. *Br J Pharmacol* 2010;160:1234-42.
 69. Hu K, Gaudron P, Ertl G. Long-term effects of beta-adrenergic blocking agent treatment on hemodynamic function and left ventricular remodeling in rats with experimental myocardial infarction: importance of timing of treatment and infarct size. *J Am Coll Cardiol* 1998;31:692-700.
 70. Zaragoza C, Gomez-Guerrero C, Martin-Ventura JL, Blanco-Colio L, Lavin B, Mallavia B, Tarin C, Mas S, Ortiz A, Egido J. Animal models of cardiovascular diseases. *J Biomed Biotechnol* 2011;2011:497841.
 71. Feng Y, Chen F, Ma Z, Dekeyzer F, Ting Y, Liu Y, Xia Q, Yu J, Zhang J, Oyen R, Ni Y. Therapeutic effects of cannabidiol on acute reperfused myocardial infarction in rabbits: evaluated with 3.0T cardiac MRI and histopathology. *Heart* 2013. [Epub ahead of print].
 72. Bergamaschi MM, Queiroz RH, Zuairi AW, Crippa JA. Safety and side effects of cannabidiol, a Cannabis sativa constituent. *Curr Drug Saf* 2011;6:237-49.
 73. Stanley CP, Hind WH, O'Sullivan SE. Is the cardiovascular system a therapeutic target for cannabidiol? *Br J Clin Pharmacol* 2013;75:313-22.
 74. Durst R, Danenberg H, Gallily R, Mechoulam R, Meir K, Grad E, Beeri R, Pugatsch T, Tarsish E, Lotan C. Cannabidiol, a nonpsychoactive Cannabis constituent, protects against myocardial ischemic reperfusion injury. *Am J Physiol Heart Circ Physiol* 2007;293:H3602-7.

Cite this article as: Feng Y, Bogaert J, Oyen R, Ni Y. An overview on development and application of an experimental platform for quantitative cardiac imaging research in rabbit models of myocardial infarction. *Quant Imaging Med Surg* 2014;4(5):358-375. doi: 10.3978/j.issn.2223-4292.2013.09.01